Modelling Contactless Ultrasound Treatment in a DC Casting Launder

Christopher Beckwith[a], Georgi Djambazov[a], Koulis Pericleous[a]

[a]Computational Science and Engineering Group, University of Greenwich, 30 Park Row, London SE10 9LS, UK

Abstract

Ultrasonic processing can be performed without a vibrating probe by electromagnetic induction with a suitable frequency where resonance conditions can be established. This contactless method is suitable for high-temperature or reactive metal alloys providing purity of the melt and durability of the equipment. Hydrogen bubbles coming out of solution grow by rectified diffusion, and larger bubbles escape from the top surface leading to degassing. Violent collapses of the remaining smaller bubbles help grain refinement. In this study, the application of a contactless 'top-coil' device to continuous casting via a launder is considered. Resonance is achieved by the positioning of baffles on either side of the coil. Electromagnetic forces also cause strong stirring, increasing residence time. The process is modelled using time domain and frequency domain methods, and results for the proposed setup are compared with data obtained for the immersed sonotrode. Accuracy and sensitivity to process and model parameters are discussed.

Keywords: Ultrasonic melt processing, numerical modelling, acoustic cavitation, acoustic resonance

1. Introduction

Techniques of improving the quality of light alloy metal billets are of high importance, as reducing trapped hydrogen through degassing, grain refinement, and dispersion of metal clusters have been linked with improvements in mechanical properties including tensile strength and ductility [1]. One such method that has been the subject of a significant amount of recent research is the application of ultrasound (UST) while the melt is still in its liquid phase before casting [2]. Traditionally this is performed with the use of an immersed mechanical vibrating sonotrode [2,3], and the high acoustic pressures directly next to the sonotrode surface result in the rapid growth and then collapse of bubbles through inertial cavitation. Unfortunately, inertially cavitating bubbles attenuate the sound field through thermal and viscous losses, in addition to acoustic radiation, which prevents cavitation from happening further away from the sonotrode surface. An alternative approach which has been the subject of recent research has been to replace the mechanical sonotrode with an AC induction coil [1,4–6]. This approach relies on resonance to build suitable pressures, and as a result can trigger cavitation deep into the melt, far away from the liquid surface. This could have a number of advantages, including the repositioning of the active zone for maximum processing efficiency (for example, just above the liquid-solid interface during casting, or through the creation of multiple active zones at the antinodes of a standing wave). This is in addition to other, already well established benefits of contactless processing which include the reduction of contamination due to sonotrode erosion, which eventually also results in reduced cost as traditional processing requires frequent sonotrode tip replacements [6]. In addition, contactless treatment also allows for the processing of high temperature (Ni, Fe, Cu) or reactive (Ti, Zr) melts which cannot be processed using a mechanical sonotrode. However, existing work mostly implements contactless UST in small scale experiments in a crucible, and work implementing the treatment in a practical casting process is limited. One study [4] performed initial numerical simulations demonstrating how contactless UST might work with the coil placed directly in the hot top of a DC caster, and showed that it was

possible to establish a fixed resonant frequency during casting, due to the impedance mismatch at the liquid-solid interface. Electromagnetic stirring then provides suitable mixing, transporting dendrite fragments which might lead to an evenly refined microstructure.

An alternative to processing directly on the hot top is to instead process further up in the launder. Previously, this has been investigated [3,7,8] for a mechanical sonotrode, and microstructure grain analysis has shown that this approach can result in more evenly refined grains. Processing in the launder is also less prone to macrosegregation caused by the acoustic streaming jet, and could potentially also be induced by the similar electromagnetic jet induced with the contactless method.

This work attempts to develop this idea further, with full 3D simulations of the fluid flow and solidification, and for the first time attempting to apply contactless UST further up in the casting process, directly in the launder instead of in the hot top.

2. Problem Description

DC casting of aluminium alloy billets has been carried out at the Advanced Metal Casting Centre (AMCC) of the Brunel Centre of Advanced Solidification Technology (BCAST). These experiments have so far used mechanical sonotrodes, as described in Figure 1a. These casts used AA6XXX series aluminium with an addition of 0.25 wt% Zr but without the addition of an AlTiB grain refiner. The diameter of the cast billets measured 152mm. Results from these experiments have previously been presented in [8] with a 5-kW magnetostrictive transducer (Reltec) driven at 17.3kHz used to power the sonotrode, which has a diameter of 40mm. The sonotrode tip was immersed 12mm below the melt surface, oscillating with a peak-to-peak amplitude of 30µm. Grain analysis showed that by applying UST in the launder, grain size decreased twofold and the presence of feathery grains was suppressed. The presence of partitions in the launders was also linked with increased acoustic pressures and more efficient UST, with the maximum acoustic pressure being twice as high as that without partitions, and RMS pressures increasing by 50%. This was linked with an additional grain refinement of approximately 10% compared to the same experiments without partitions.

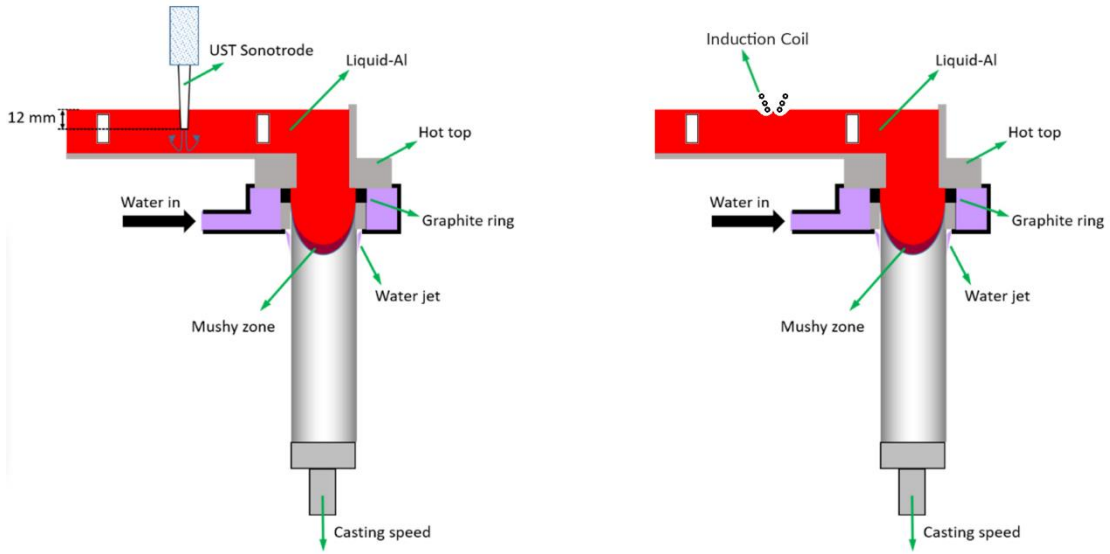

Figure 1: (a) A typical setup for ultrasonic melt treatment in the launder using a mechanical sonotrode. (b) The alternative setup uses an AC induction coil. Partitions are placed in the launder for both cases.

For simulations investigating the potential effect of replacing the sonotrode with an AC Induction coil, the partitions also increase the potential for resonance by adding additional geometry for sound

reflection, as the location of these partitions can be modified to target particular acoustic frequencies. Numerical simulations are carried out assuming the same experimental conditions and partition configuration as the experiments with a sonotrode, but with the induction coil immersed into the liquid as shown in Figure 1b.

3. Modelling Approach

A number of authors have presented models for the frequency domain calculation of the acoustic field including the effect of inertially cavitating bubbles [9–11]. In our previous paper [5], the model of [9] was modified and a nonlinear Helmholtz equation for cavitation problems including the effect of a background source term $F^{\star}$ representing the Lorentz force was obtained. A description of the method is given in this section, but for a full description including derivation, please see the cited work. The equations governing the propagation of the sound field are given in equations (1)-(2), where P represents the complex acoustic pressure field, and k_m^2 is a modified wave number due to the attenuation and change of speed of sound that exists in the presence of inertially cavitating bubbles. The nonlinear Helmholtz equation includes terms which allow for the variation in density at material boundaries (e.g. containing walls), in addition to the density change that occurs during solidification.

$$\nabla\left(\frac{1}{\rho}\nabla P - \frac{F^{\star}}{\rho}\right) + \frac{k_m^2}{\rho}P = 0 \tag{1}$$

$$k_m^2 = \left(\frac{\omega}{c}\right)^2 - \frac{\mathcal{A}(P)}{|P|} - i\frac{\mathcal{B}(P)}{|P|} \tag{2}$$

The dispersion coefficients $\mathcal{A}$ and $\mathcal{B}$ can then be calculated using Equation (3) [9], which considers only the change in void faction over the last acoustic period.

$$\mathcal{A} = -\frac{\rho_l \omega^2}{\pi}\int_0^{2\pi}\frac{\partial\beta}{\partial\tau}\sin\tau\, d\tau, \quad \mathcal{B} = -\frac{\rho_l \omega^2}{\pi}\int_0^{2\pi}\frac{\partial\beta}{\partial\tau}\cos\tau\, d\tau \tag{3}$$

Where $\beta = 4/3\pi r^3 N$ is the void fraction and N is the number of bubbles. The void fraction must be computed with a bubble dynamics simulation, and many choices could be suitable for solving the time evolution of bubbles, for example [12,13]. Here, the Keller-Miksis Equation (KME) as given in [14] is used due to first order compressibility and acoustic radiation terms and is shown here in Equation (4).

$$\left(1-\frac{\dot{R}}{C}\right)R\ddot{R} + \frac{3}{2}\dot{R}^2\left(1-\frac{\dot{R}}{3c}\right) = \frac{1}{\rho_l}\left(1+\frac{\dot{R}}{c}+\frac{R}{c}\frac{d}{dt}\right)[p_l - p(t)] \tag{4}$$

Where p_l represents the liquid pressure at the liquid gas interface and is defined by Equation (5), where σ_e is the surface tension, μ is the liquid viscosity, and p_g is the pressure in the gas at the interface, which can be assumed to follow the adiabatic equation of state [15] given by Equation (6).

$$p_l = p_g - \frac{2\sigma_e}{R} - \frac{4\mu\dot{R}}{R} \tag{5}$$

$$p_g = p_{g0}\left(\frac{R_0}{R}\right)^{3\gamma} \tag{6}$$

Here, $\gamma = 1.4$ is the polytropic exponent, and p_{g0} the initial gas pressure in the bubble. A background pressure $p(t) = p_0(1 - A\,sin(\omega t))$ accounts for both the sinusoidal acoustic pressure with dimensionless amplitude A, and atmospheric pressure. It is important to run the single bubble

model for more than one acoustic period so that simulation can converge to a harmonic solution, and the number of cycles needed increases with frequency and driving amplitude [9]. In the simulations in this paper, 500 cycles are chosen as the cut-off point at which if a harmonic solution has not been obtained, interpolation with cubic splines is used instead.

N is assumed to be a smoothed stepwise function $W(|P|)$ centred on the Blake pressure, with a smoothing distance equal to $P_{blake} - P_{rd}$, the difference between the Blake threshold and the rectified diffusion threshold, the acoustic pressure required for bubbles to begin growing. Under this pressure, hydrogen bubbles begin dissolving back into solution and do not significantly influence the acoustic field. Assuming that the driving frequency is far from the bubble resonant frequency, which is generally the case in metal processing. The resulting threshold is given by Equation (7) [5], where C_i is the concentration of hydrogen in the bulk fluid, C_0 is the saturation concentration, η is the polytropic coefficient.

$$P_{rd}^2 = \frac{(\rho R_0^2 \omega_0^2)^2[(1-\omega^2/\omega_0^2)^2 + b^2(\omega^2/\omega_0^2)](1 + 2\sigma/R_0 P_\infty - C_i/C_0)}{(3+4K)(C_i/C_0) - \left\{\left[\frac{3}{4}(\eta-1)(3\eta-4)\right] + (4-3\eta)K\right\}(1 + 2\sigma/R_0 P_\infty)} \quad (7)$$

For the fluid flow simulation, Equations (8) and (9) describe the continuity and momentum equations. An additional term F_s is included to model the additional stirring due to the influence of a background field. For the top mounted induction coil, this term represents the induced Lorentz forces, the mean component of which drives the main fluid flow. For an immersed sonotrode, this term can be used to represent acoustic streaming, which has been shown in previous work [3,7,8]. The Lorentz forces induced by the coil are calculated from a separate simulation using Comsol's Magnetic Fields solver. Solidification at the mould is then included through the use of a continuum approach described in [16] and previously used in [7]. The continuum approach adds a Carman–Kozeny momentum sink term S_d that forces the fluid velocity to the background velocity v_{ref}. This was implemented using a custom OpenFOAM solver based on the included "buoyantPimpleFoam" solver (a combination of the PISO and SIMPLE algorithms). The electromagnetic source terms were exported from Comsol in CSV format and then interpolated onto the OpenFOAM mesh.

$$\nabla \cdot v = 0 \quad (8)$$

$$\rho_0 \frac{\partial v}{\partial t} + \rho_0 \nabla \cdot (vv) = -\nabla p + \mu_0 \nabla^2 v + \rho_0 g \beta_T (T - T_{ref}) + S_d + F_s \quad (9)$$

Where ρ_0 and μ_0 are the fluid density and the dynamic viscosity. Turbulence is included in the model, using the k-Omega-SST turbulence model. The system is closed by the energy balance, as given in Equation (10).

$$\rho c_p \frac{\partial T}{\partial t} + \rho c_p \nabla \cdot (vT) = \nabla \cdot (k \nabla T) - \rho_0 L_f \left[\frac{\partial g_l}{\partial t} + \nabla \cdot (v g_l)\right] \quad (10)$$

where $c_p$is the specific heat, T is the temperature, and k is the thermal conductivity, L_f the latent heat of fusion, and g_l the volume fraction of liquid. In the slurry, the effective dynamic viscosity μ_{eff} can be calculated from the Stefanescu formula [18,19] given in Equations (11, 12), where μ_l is the liquid viscosity, f_s is the solid fraction, and f_c is the dendrite coherency point, chosen to be 0.3.

$$\mu_{eff} = \mu_l \left(\frac{1}{1 - F_\mu f_s / f_c}\right)^2 \quad (11)$$

$$F_{\mu} = 0.5 - (1/\pi)\tan^{-1}\big(100(f_s - f_c)\big) \tag{12}$$

At the water spray, the heat transfer can be described by a Fourier boundary condition with a heat flux function depending on the average temperature $\bar{T}$ between the surface of the billet and the bulk fluid [21]. Including the effect of nucleate boiling above a critical point $q_c = 3910\Delta T^{2.16}$ the heat transfer coefficient takes the form of Equation (13).

$$h_c = \begin{cases} [-1.67 \times 10^5 + 704\bar{T}] \cdot Q'^{1/3}, & \text{if } q_c \geq q_i \\ [-1.67 \times 10^5 + 704\bar{T}] \cdot Q'^{1/3} + \dfrac{20.8(\Delta T_x)^3}{\Delta T}, & \text{if } q_c < q_i \end{cases} \tag{13}$$

At the free surface, a surface radiation boundary condition is used and is given by Equation (14), where $\epsilon = 0.3$ is the surface emissivity and $\sigma = 5.6708 \times 10^{-8}$ the Stefan–Boltzmann constant.

$$\nabla \mathrm{T} = \frac{\epsilon\sigma\big(T_{\mathrm{amb}}^4 - T^4\big)}{k} \tag{14}$$

4. Results

Following the solution procedure described in [5], target acoustic Eigenfrequencies are first calculated from a linear model (achieved by setting N=0), and are then used as an initial guess for the resonant frequency including the effect of cavitation. The frequency is then adjusted until resonance is achieved in the non-linear case. Target frequencies were taken only if they were below 30kHz, to target specific modes that could be obtainable by the AC coil. A full list of material properties for the liquid aluminium is given in Table 1, and the properties of the copper induction coil are given in Table 2.

Table 1. Model properties of liquid aluminium. Properties obtained from [15].

Electrical Conductivity (S/m)	4e6
Relative permeability	1
Relative permittivity	1
Casting velocity (m s^{-1})	0.0023
Inlet temperature (K)	1003.15
Liquidus temperature (K)	929.2
Solidus temperature (K)	757.4
Latent Heat (J kg^{-1})	375696.0
Density (kg m^{-3})	2375
Speed of sound (m s^{-1})	4600
Thermal expansion coefficient (K^{-1})	2.3×10^{-5}
Kinematic viscosity (m^2s^{-1})	5.5×10^{-7}

Table 2. Properties of the copper induction coil.

Electrical Conductivity (S/m)	5.998e7
Relative permeability	1
Relative permittivity	1
Density (Kg m^{-3})	8700

In the acoustic simulation, a sound soft ($P = 0$) boundary condition is used on the top surface, and sound hard boundaries are used elsewhere. At the inlet and outlet of the launder, a perfectly matched layer was used to prevent reflections, in an attempt to focus on resonant modes present

due to partitions and to prevent unnatural resonant frequencies that might occur due to not simulating the entire launder. Figure 2 shows two chosen eigenfrequencies for the launder with partitions. The two Eigenfrequencies occurred at 21564Hz and 23862Hz, corresponding to electrical frequencies of 10782Hz and 11931Hz and high pressure regions were located close to the partitions. For the rest of the results in this work, the 21564Hz mode will be the target mode that we will use.

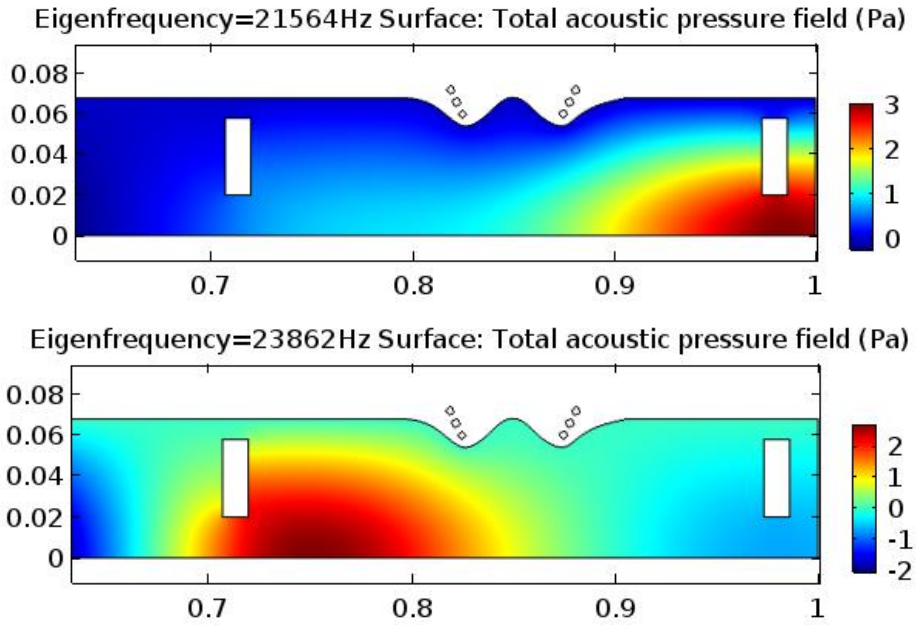

Figure 2: Obtained Eigenfrequencies from linear theory potentially obtainable by the AC coil. (a) (b) The alternative setup uses an AC induction coil. Partitions are placed in the launder for both cases.

The nonlinear Helmholtz solver is then used to compute the acoustic field in the presence of cavitating bubbles. The properties of these hydrogen bubbles are given in Table 3. Due to the reduction in speed of sound that occurs with an increase in bubble volume fraction, the resonant frequency is slightly lower than that of the eigenfrequency study, and the closest frequency is calculated to be 21320Hz, a shift of 244Hz. Results for this case are shown in Figure 3b. Peak pressures induced by the coil were approximately 180kPa, well above the threshold for cavitation for 10 micron hydrogen bubbles in liquid aluminium (calculated to be approximately 154kPa [5]). The traditional mechanical sonotrode is capable of reaching much higher pressures, up to 600kPa directly below the sonotrode surface, but the active region is isolated to the area directly under the sonotrode, with acoustic shielding preventing higher pressures elsewhere in the domain. This can be seen in Figure 3a. The top coil by comparison resulted in an active zone much deeper below the surface, located in the gap between the downstream partition and the base of the launder.

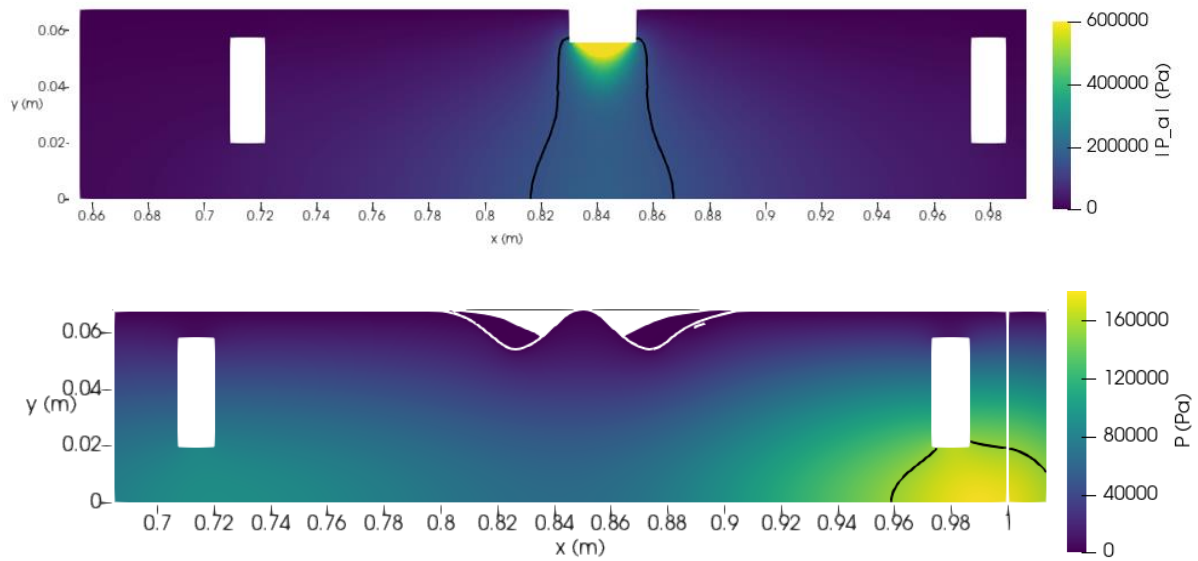

Figure 3: The induced acoustic field including the effect of inertially cavitating bubbles, using an immersed sonotrode operating at 17300Hz (a) and a top mounted induction coil operating at 10660Hz (an acoustic frequency of 21320Hz) (b). The black line in both figures indicates the active processing zone above the Blake threshold.

Table 3. Hydrogen bubble properties [15].

Bubble Density N	5e7
Surface Tension (N m^{-1})	0.860
Vapour pressure (Pa)	0
Specific Heat Capacity (J kg^{-1} K^{-1})	717
Bulk Temperature (K)	1013.15
Ambient bubble radius R_0 (m)	10×10^{-6}

Figure 4 shows the induced magnetic field from the AC induction coil at an electrical frequency of 10660Hz. The coil interacts with induction currents in the melt to repel the free surface, ensuring that no contact is made with the metal. At the electromagnetic skin layer, the magnetic flux density reaches a peak of 0.11T, comparable to that in previous work in a crucible [5]. The interacting magnetic and electric fields result in a force on the aluminium $F = J \times B$. This force has a mean component given in Figure 4b which drives the bulk fluid flow, and is used as the source term F_s in Equation (9), and a harmonic oscillating component given in Figure 4c, which is responsible for the acoustic field source term $F^{\star}$. The magnitude of the mean part was found to be lower than the amplitude of the harmonic part, with peak amplitudes of the order 2e6 and 6e6 respectively.

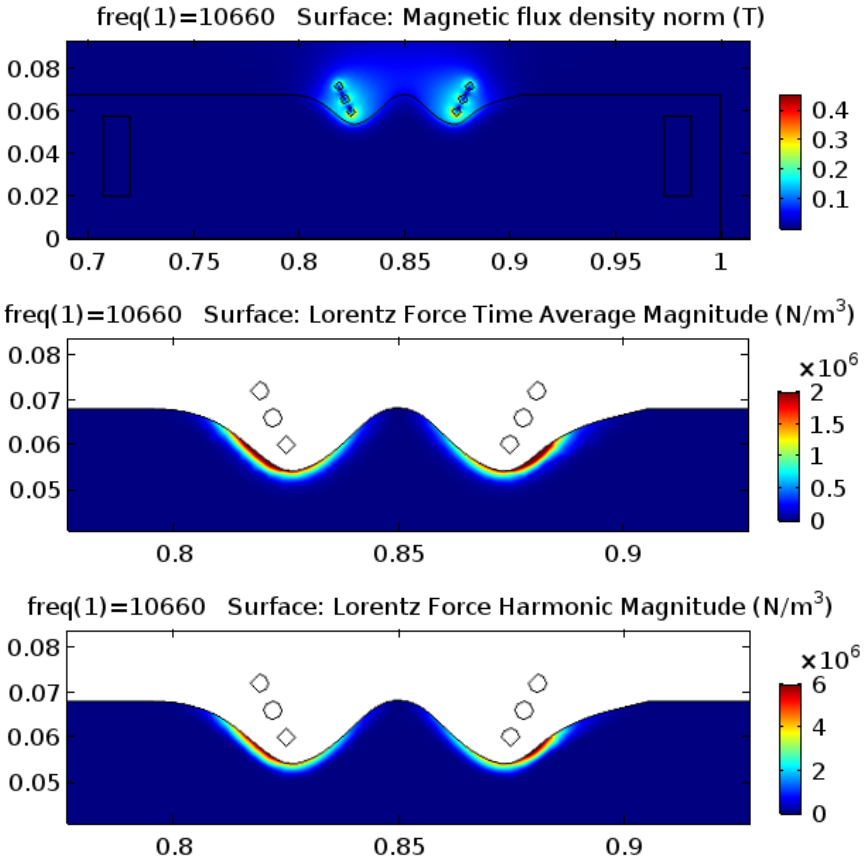

Figure 4: (a) Induced magnetic field from the AC induction coil at 10660Hz, in addition to the magnitude of the resulting mean Lorentz force (b) and harmonic component (c)

The fluid flow induced by the sonotrode reached a peak velocity of approximately 1m/s directly below the sonotrode, with the acoustic streaming jet having a velocity closer to 0.6m/s. Flow patterns for this case can be seen in Figure 5a. The top coil on the other hand, which does not rely on acoustic streaming but instead the electromagnetic Lorentz forces, reached a peak velocity of approximately 2.5m/s, 2.5x what was obtained by the sonotrode. This results in very strong mixing and is likely to result in a very even distribution of processed particles, which has previously been linked with improved uniformity in grain size across the final billet [7]. This could then further be improved by designing a geometry such that the resonant mode, and therefore the active processing region, be located to increase residence time before mixing, as in these simulations the active zone primarily acts downstream, which could limit the effectiveness of treatment. The resulting sump profile showing the solidification of the billet in the mould and temperature contours are given in Figure 5c.

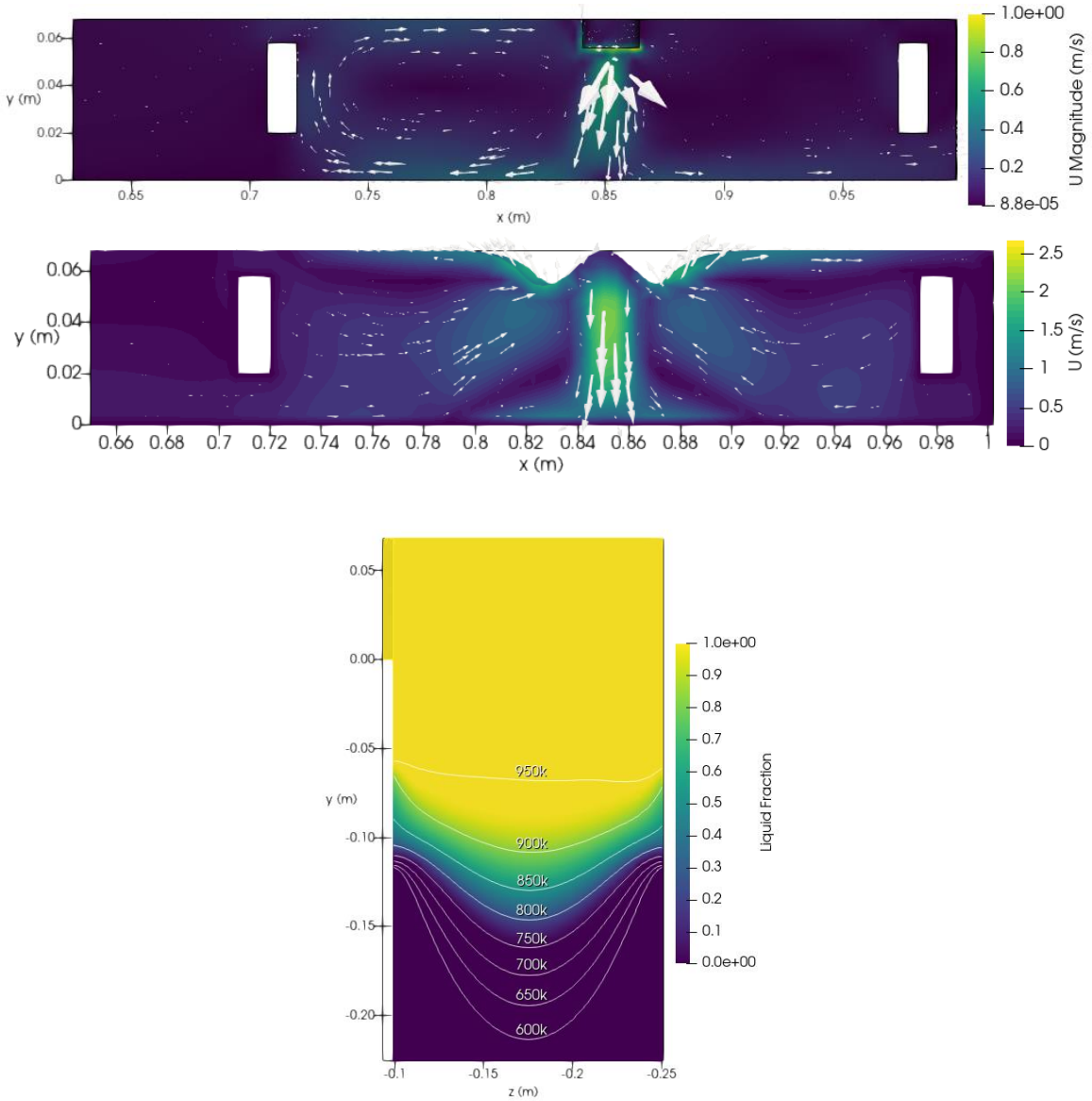

Figure 5: The fluid flow induced by the acoustic streaming generated traditional mechanical sonotrode (a), Lorentz forces generated by the induction coil (b), and the sump profile in the mould with temperature contours (c)

5. Integrated Cylindrical Vessel

An alternative geometry using a cylindrical vessel integrated into the launder is presented in this section. This concept hopes to improve the efficiency of processing by encouraging a central resonant mode, with partitions placed to restrict flow in and out of the isolated cylindrical vessel. A diagram of this concept is given in Figure 6.

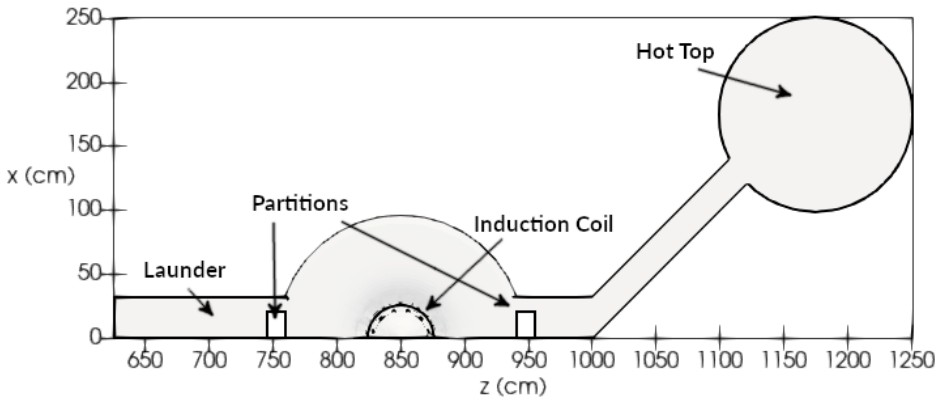

Figure 6: Launder concept which aims to improve contactless UST processing efficiency by integrating an additional cylindrical vessel into the launder.

Initial simulations were carried out on the cylindrical vessel, carried out in 3 stages. Initially, an electromagnetics solver computes the magnetic and electric fields, then the fluid flow, followed by the acoustics. For the electromagnetics and free surface model, Maxwell's equations in electromagnetic induction approximation are solved numerically via a formulation based on the electric field vectors (real and imaginary parts) and Biot-Savart integral [17]. The 3-turn top coil was modelled as 3 axisymmetric rings each carrying a current of 1700A at 14580.4Hz. This frequency was chosen as the lowest for which the periodic component of the Lorentz force induces acoustic resonance in the metal volume with a radius of 96.4 mm and a height of 100 mm. The coils are lowered from their initial positions where the lowest turn is 5 mm above the metal surface in steps of 1.25 mm and the computational mesh is deformed according to the mean pressure exerted by the Lorentz force until a total displacement of 17.5 mm (Figure 7) is reached – just before the hydrostatic pressure of the liquid metal under the deformed free surface becomes too high for the generated Lorentz force to balance. Both the mean and the periodic components of the Lorentz force vectors are saved for the next stages.

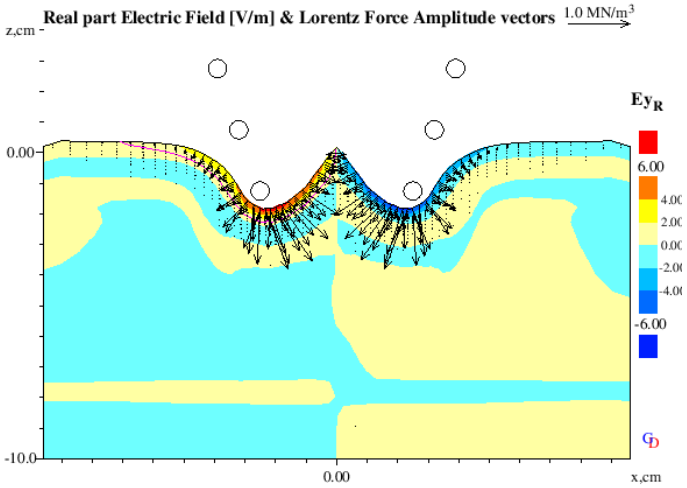

Figure 7: Vertical central cross-section of the liquid metal volume and top coil showing the deformed free surface, electric field contours and amplitude of the periodic component of the Lorentz force vectors; 'real part' means in phase with the driving coil electrical current.

The flow of the liquid metal is then caused by the mean component of the Lorentz force. Figure 8 shows the result of a CFD simulation with a k-ε turbulence model carried out in the PHYSICA code. The calculated maximum velocity in the downward jet is 0.38 m/s, comparable to typical flow patterns induced by an immersed sonotrode. This is less than the 2.5m/s jet obtained by the frequency domain simulation in the previous section, but this can largely be explained by the coil operating at 1700A as opposed to 2000A, which also reduces the induced Lorentz forces.

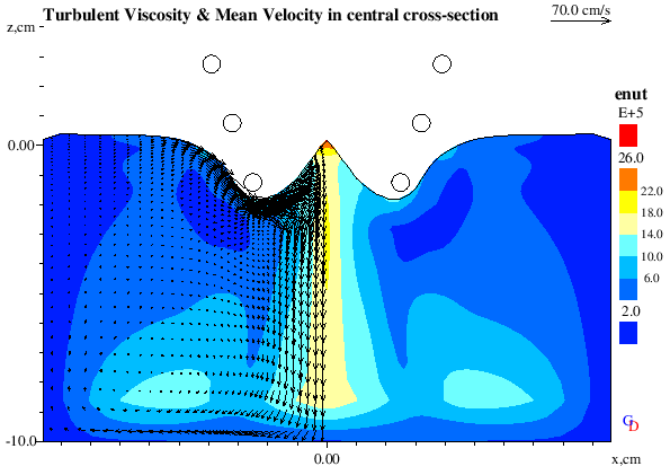

Figure 8: CFD result for the mean flow driven by the steady component of the Lorentz force; contours – turbulent viscosity, vectors – flow velocity.

Acoustic cavitation of any hydrogen bubbles formed in the melt is driven by the periodic part of the electromagnetic Lorentz force. It is simulated with a bespoke piece of software [5] capturing the time-dependent behaviour of both the acoustic field and the bubbles dispersed in the metal volume. 32366 acoustic cycles were simulated with time step 1.75×10^{-7} s, taking about 5 hours on a 32-processor workstation. The acoustic algorithm [18] needs a regular cartesian grid, so the depression of the free surface is not modelled within the acoustic part, but the total volume of liquid metal is retained. The equilibrium bubble radius, i.e. the radius without acoustic excitation, is assumed to be 7 μm and the bubble concentration is 1×10^{7} m^{-1}. Acoustically soft (zero pressure amplitude) boundary conditions were assumed on all sides of the liquid metal volume. The simulated acoustic field as shown in Figure 9 (for RMS pressure p) shows a spheroidal zone with an approximate radius of 2 cm around the centre of the domain which is above the Blake threshold for inertial cavitation (130 kPa RMS in the simulated case) and is the necessary condition for cavitation treatment of the melt. A Lorentz force frequency in the acoustic simulation was set at 29132 Hz, but its amplitude was taken from the electromagnetic results. One can see the prescribed frequency is not exactly twice the electrical (as expected theoretically) and the slight shift is needed to sustain resonance under the bubble action which alters the effective speed of sound in the liquid metal. This is important for practical applications as automatic frequency tuning will be needed.

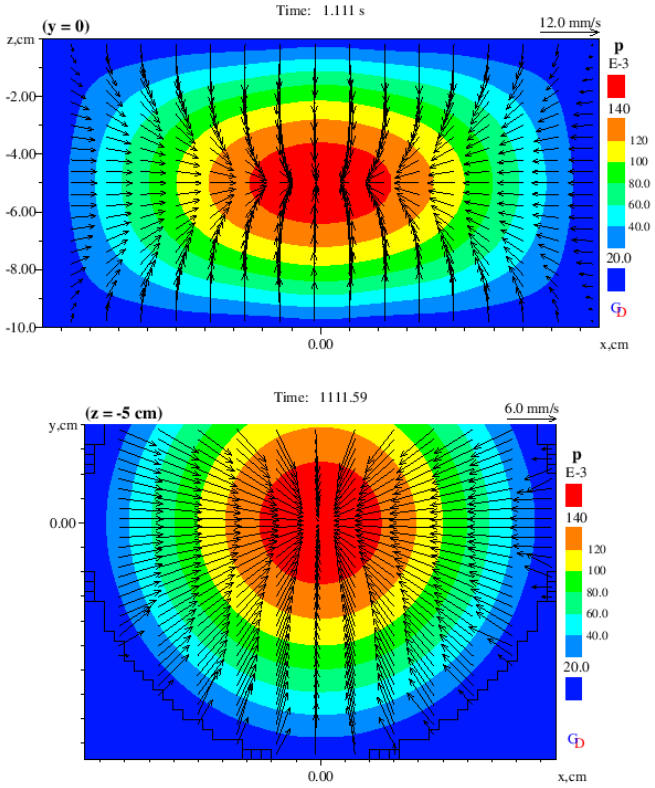

Figure 9: Vertical and horizontal sections of the acoustic cavitation field showing the RMS acoustic pressure averaged over 0.1 s just before the end of the simulated 1.11s

6. Conclusions

A coupled model for simulating the acoustic field in the presence of bubbles, electromagnetic induction from an AC coil, and fluid flow has been presented and has been applied to the potential application of contactless UST processing in the launder. It has been shown numerically that it is possible to obtain pressures required for processing as the Blake threshold was exceeded deep into the launder close to the partitions. This mode was obtained at 10660Hz electrical frequency, corresponding to an acoustic frequency of 21320Hz, which is obtainable by the coil. In addition, induced flow velocities were 2.5x higher in the launder when using the Lorentz force, as opposed to traditional UST processing with a mechanical sonotrode. This could have benefits for enhanced mixing and could be used to evenly distribute processed particles that would result in an even distribution of refined grains in the final billet. However, as this was not tested further theoretical and experimental work needs to be carried out to determine the exact effect that this will have on grain refinement.

In addition, an alternative launder concept has been suggested that might be better suited for contactless UST. The new concept integrates a cylindrical vessel into the launder, and a resonant mode can then be calculated which results in a large active zone directly in the middle of the vessel. Induced flow velocities for this system are comparable to that obtained by traditional UST with a sonotrode but needed a higher acoustic frequency of 29132Hz to obtain.

References

1. Dybalska, A.; Caden, A.; Griffiths, W.D.; Nashwan, Z.; Bojarevics, V.; Djambazov, G.; Tonry, C.E.H.; Pericleous, K.A. Enhancement of Mechanical Properties of Pure Aluminium through Contactless Melt Sonicating Treatment. *Materials* **2021**, *14*, 4479, doi:10.3390/ma14164479.

2. Eskin, G.I.; Eskin, D.G. *Ultrasonic Treatment of Light Alloy Melts, Second Edition*; CRC Press, 2014; ISBN 978-1-4665-7798-5.
3. Subroto, T.; Eskin, D.G.; Beckwith, C.; Skalicky, I.; Roberts, D.; Tzanakis, I.; Pericleous, K. Structure Refinement Upon Ultrasonic Melt Treatment in a DC Casting Launder. *JOM* **2020**, *72*, 4071–4081, doi:10.1007/s11837-020-04269-3.
4. Tonry, C.E.H.; Bojarevics, V.; Djambazov, G.; Pericleous, K. Contactless Ultrasonic Treatment in Direct Chill Casting. *JOM* **2020**, *72*, 4082–4091, doi:10.1007/s11837-020-04370-7.
5. Beckwith, C.; Djambazov, G.; Pericleous, K.; Tonry, C. Comparison of Frequency Domain and Time Domain Methods for the Numerical Simulation of Contactless Ultrasonic Cavitation. *Ultrasonics Sonochemistry* **2022**, *89*, 106138, doi:10.1016/j.ultsonch.2022.106138.
6. Pericleous, K.; Bojarevics, V.; Djambazov, G.; Dybalska, A.; Griffiths, W.D.; Tonry, C. Contactless Ultrasonic Cavitation in Alloy Melts. *Materials* **2019**, *12*, 3610, doi:10.3390/ma12213610.
7. Beckwith, C.; Djambazov, G.; Pericleous, K.; Subroto, T.; Eskin, D.G.; Roberts, D.; Skalicky, I.; Tzanakis, I. Multiphysics Modelling of Ultrasonic Melt Treatment in the Hot-Top and Launder during Direct-Chill Casting: Path to Indirect Microstructure Simulation. *Metals* **2021**, *11*, 674, doi:10.3390/met11050674.
8. Subroto, T.; Eskin, D.G.; Beckwith, C.; Roberts, D.; Tzanakis, I.; Pericleous, K. Effect of Flow Management on Ultrasonic Melt Processing in a Launder upon DC Casting. In Proceedings of the Light Metals 2022; Eskin, D., Ed.; Springer International Publishing: Cham, 2022; pp. 649–654.
9. Trujillo, F.J. A Strict Formulation of a Nonlinear Helmholtz Equation for the Propagation of Sound in Bubbly Liquids. Part I: Theory and Validation at Low Acoustic Pressure Amplitudes. *Ultrasonics Sonochemistry* **2018**, *47*, 75–98, doi:10.1016/j.ultsonch.2018.04.014.
10. Louisnard, O. A Simple Model of Ultrasound Propagation in a Cavitating Liquid. Part I: Theory, Nonlinear Attenuation and Traveling Wave Generation. *Ultrasonics Sonochemistry* **2012**, *19*, 56–65, doi:10.1016/j.ultsonch.2011.06.007.
11. Jamshidi, R.; Brenner, G. Dissipation of Ultrasonic Wave Propagation in Bubbly Liquids Considering the Effect of Compressibility to the First Order of Acoustical Mach Number. *Ultrasonics* **2013**, *53*, 842–848, doi:10.1016/j.ultras.2012.12.004.
12. Plesset, M.S. The Dynamics of Cavitation Bubbles. *Journal of Applied Mechanics* **1949**, *16*, 277–282, doi:10.1115/1.4009975.
13. Löfstedt, R.; Barber, B.P.; Putterman, S.J. Toward a Hydrodynamic Theory of Sonoluminescence. *Physics of Fluids A: Fluid Dynamics* **1993**, *5*, 2911–2928, doi:10.1063/1.858700.
14. Keller, J.B.; Miksis, M. Bubble Oscillations of Large Amplitude. *The Journal of the Acoustical Society of America* **1980**, *68*, 628–633, doi:10.1121/1.384720.
15. Harkin, A.; Nadim, A.; Kaper, T.J. On Acoustic Cavitation of Slightly Subcritical Bubbles. *Physics of Fluids* **1999**, *11*, 274–287, doi:10.1063/1.869878.
16. Voller, V.R.; Prakash, C. A Fixed Grid Numerical Modelling Methodology for Convection-Diffusion Mushy Region Phase-Change Problems. *International Journal of Heat and Mass Transfer* **1987**, *30*, 1709–1719, doi:10.1016/0017-9310(87)90317-6.
17. Djambazov, G.; Bojarevics, V.; Pericleous, K.; Croft, N. Finite Volume Solutions for Electromagnetic Induction Processing. *Applied Mathematical Modelling* **2015**, *39*, 4733–4745, doi:10.1016/j.apm.2015.03.059.
18. Lebon, G.S.B.; Tzanakis, I.; Djambazov, G.; Pericleous, K.; Eskin, D.G. Numerical Modelling of Ultrasonic Waves in a Bubbly Newtonian Liquid Using a High-Order Acoustic Cavitation Model. *Ultrasonics Sonochemistry* **2017**, *37*, 660–668, doi:10.1016/j.ultsonch.2017.02.031.